1. GENERAL DESIGN AND LAYOUT

1.1 Scope of This Report

The aim of this Design Report is to present as complete a design as possible of the superconducting accelerator to be built at the Fermi National Accelerator Laboratory. There have been many significant advances in design of the accelerator in the last year and it is useful to record these advances in order to put these problems behind us and continue the work. It is also useful to make a coherent presentation of the plans in order to integrate the design.

In addition, in the last few years, the possible long-range scope of the accelerator has enlarged greatly with its suggested applications for colliding beams, either proton-antiproton or proton-proton. These new applications have prompted considerable new design effort, the details of which will be documented here. Finally, it is our hope that this report will have some value for reference by the Fermilab people working on the project.

All these aims can best be met by a report in considerably greater technical depth than has been exhibited in most previous design reports on the Fermilab superconducting-accelerator work. Our objective in this report is to lay out the design in as much detail as possible. The history of the Fermilab effort in this field and the use of this accelerator for high-energy physics research have been discussed in adequate detail in the previous reports and are not included in this report.

1.2 Design Goals

The ultimate goal of the superconducting ring is to extend research at Fermilab to higher energy. The field strength that has been achieved in superconducting-magnet development implies a fixed-target physics program at twice the energy now available. The potential exists for colliding-beam experiments at very high energy, either with the new ring itself for antiprotons on protons or with the new accelerator and the Main Ring for protons on protons. A significant interim goal is to reduce the power demands and costs of present operation in the 400-GeV range by sharing the acceleration cycle between the two rings.

This will be the first large superconducting-magnet synchrotron-storage ring to be completed. The development work has broken new technical ground in a number of ways. Real gains have been made in the areas of superconductive stability, quality control of superconducting materials, the engineering of large cryogenic systems, and production of extremely precise magnetic fields in the face of large Lorentz forces on conductors and of large temperature variations.

At this time, there are still questions outstanding concerning production of high-quality superconducting magnets in large quantity, concerning operation of very large cryogenic systems, and concerning quenching of magnets by particle beams. There have been successes in the Fermilab work on these problems, but continued effort is required.

Specifications of the superconducting accelerator as a fixed-target accelerator, as a $\bar{p}p$ collider, and as a pp collider are given in Tables 1-I, 1-II, and 1-III respectively.

Table 1-I. Fixed-Target Accelerator Specifications.

Peak energy	800-1000 GeV
Intensity	$> 2\times10^{13}$ ppp
Injection energy	150 GeV, single turn
Repetition rate	1-2 cycles/min
Acceleration rate	50-75 GeV/s
Flattop time	Variable to dc
Extraction	Slow: 1 to 10 s Fast: 1 ms
Beam abort system	Single - turn extraction

Table 1-II. $\bar{p}p$ Collider Specifications.

Peak energy	(800-1000 GeV) × (800-1000 GeV)
No. of bunches in each beam	1-12
Luminosity/bunch	$1-8\times10^{28}\,cm^{-2}\,sec^{-1}$
No. of interaction region	1-2
Longitudinal space for detector	> 10 m
Vacuum in warm regions	$< 10^{-8}$ Torr
Storage time	> 3 h
Injection	Forward and backward, single bunch
RF	Independent phase adjustments on $\bar{p}$ and p bunches
Abort	Forward and backward

Table 1-III. pp Collider Specifications.

Peak energy	Main Ring: 150-200 GeV Superconducting Ring: 800-1000 GeV
Intensity of each beam	$> 2\times10^{13}$
Luminosity	$> 2\times10^{30}\,cm^{-2}\,sec^{-1}$
No. of interaction region	1
Longitudinal space for detector	> 10 m
Storage time	$> \frac{1}{2}$ h
Injection and acceleration in Main Ring	Forward and backward

1.3. Layout

The layout is constrained by the requirement that it should be installed in the Main-Ring tunnel. The ring will be located directly underneath the Main Ring and will have six long straight sections coinciding with those of

the Main Ring. Figure 1-1 is a Main-Ring tunnel cross section showing the locations of the superconducting magnets and their utilities.

All beam-manipulation functions must be laid out in the six long straight sections, which will have warm beam pipes. These functions are:

1. Injection; p forward and $\bar{p}$ backward at an energy greater than 100 GeV.
2. Acceleration; in addition to accelerating a forward p beam at more than 50 GeV/s, the rf system is to be capable of accelerating simultaneously a forward p beam and a backward $\bar{p}$ beam with independently adjustable phases for the two beams.
3. Extraction of the forward p beam; a resonant-extraction system that can provide both slow (1 to 10 s) and fast (1-ms) beam spills into the present switchyard.
4. Abort; must be able to abort both the forward p beam and the backward $\bar{p}$ beam with near 100% efficiency.
5. Colliding-beam region; at least one long straight section will be dedicated to colliding beams (both $\bar{p}p$ and pp). This will be the location of the principal detector for colliding-beams experiments.
6. Scraper-shield; to obtain the required high efficiency of aborting and extraction, it is necessary that a scraper-shield be interlaced into a local orbit bump generated by conventional magnets that can withstand high radiation levels. Lower-energy charged

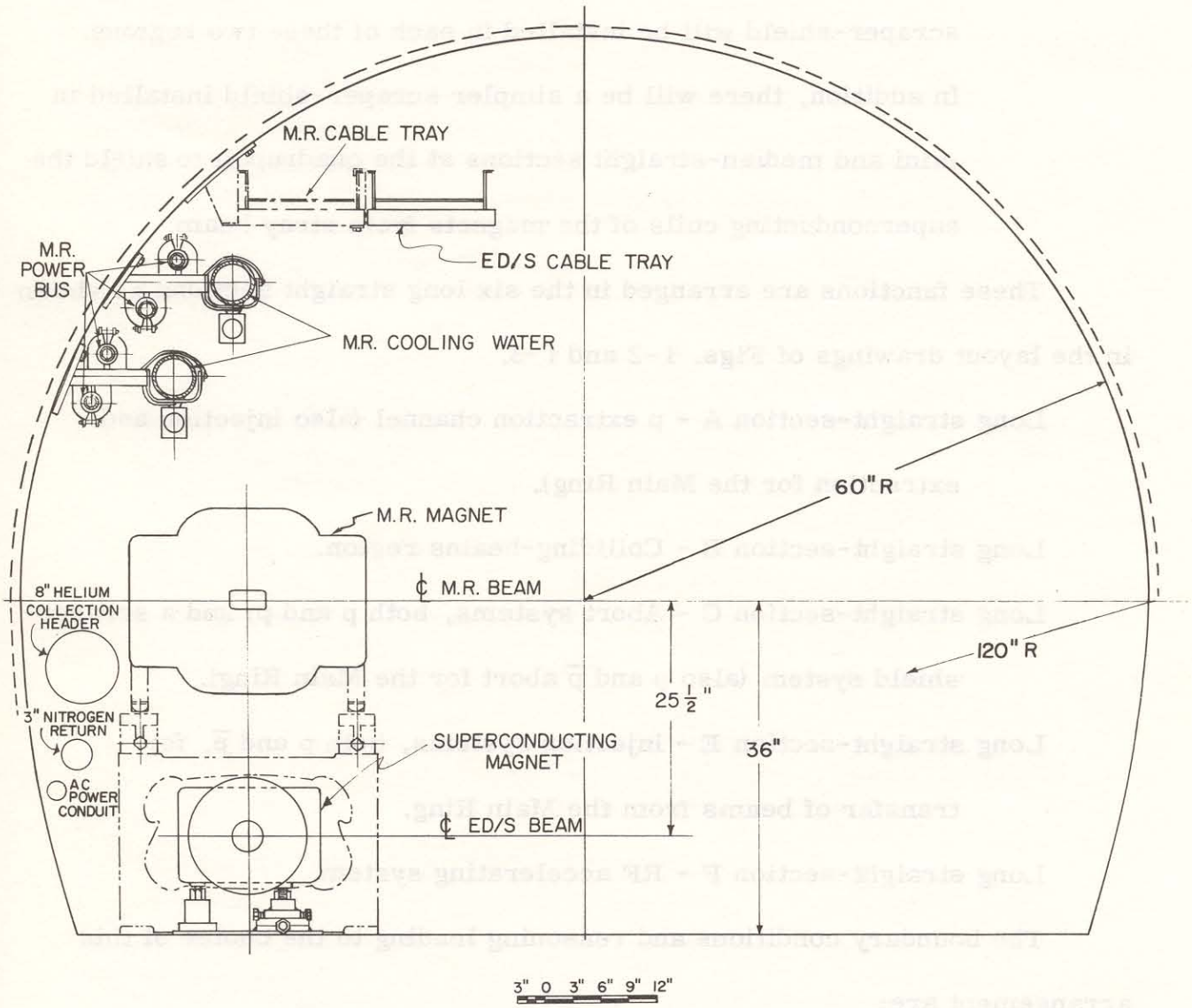

Fig. 1-1. Cross section of the accelerator tunnel.

particles in the nuclear cascade will be swept away by the magnetic field. The two high-radiation regions are the extraction-septum region and the beam-abort region. An elaborate scraper-shield will be installed in each of these two regions. In addition, there will be a simpler scraper-shield installed in mini and median-straight sections at the quadrupole to shield the superconducting coils of the magnets from stray beam.

These functions are arranged in the six long straight sections as shown in the layout drawings of Figs. 1-2 and 1-3.

Long straight-section A - p extraction channel (also injection and extraction for the Main Ring).

Long straight-section B - Colliding-beams region.

Long straight-section C - Abort systems, both p and $\bar{p}$; and a scraper-shield system (also p and $\bar{p}$ abort for the Main Ring).

Long straight-section E - Injection systems, both p and $\bar{p}$, for transfer of beams from the Main Ring.

Long straight-section F - RF accelerating system.

The boundary conditions and reasoning leading to the choice of this arrangement are:

(i) Because of the location of the existing RF Building, F is the natural choice for the r f system. Furthermore, the coupling between the Main-Ring and superconducting-ring rf systems is such that as the demand

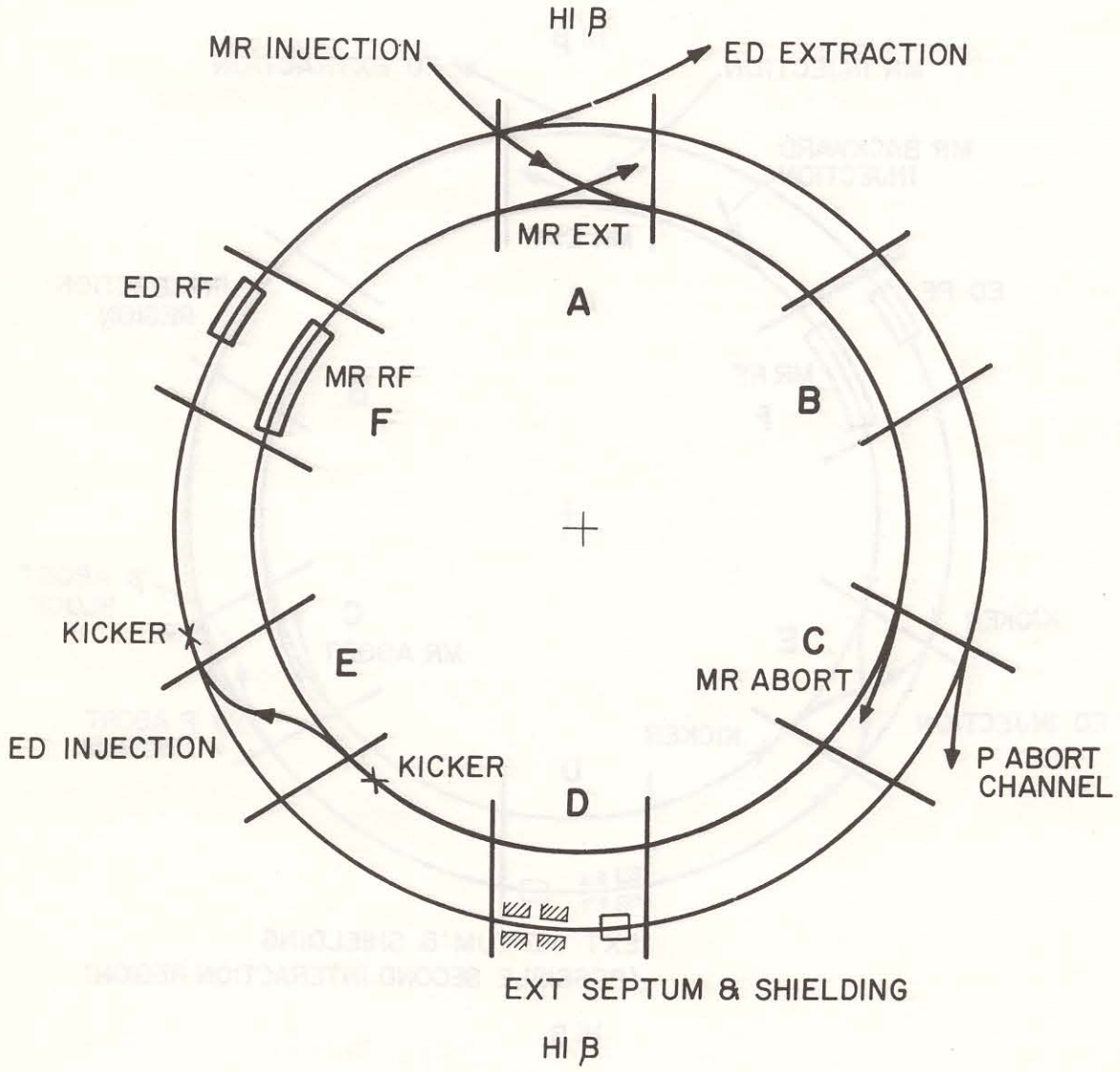

Fig. 1-2. Use of the six long straight sections in the fixed target mode.

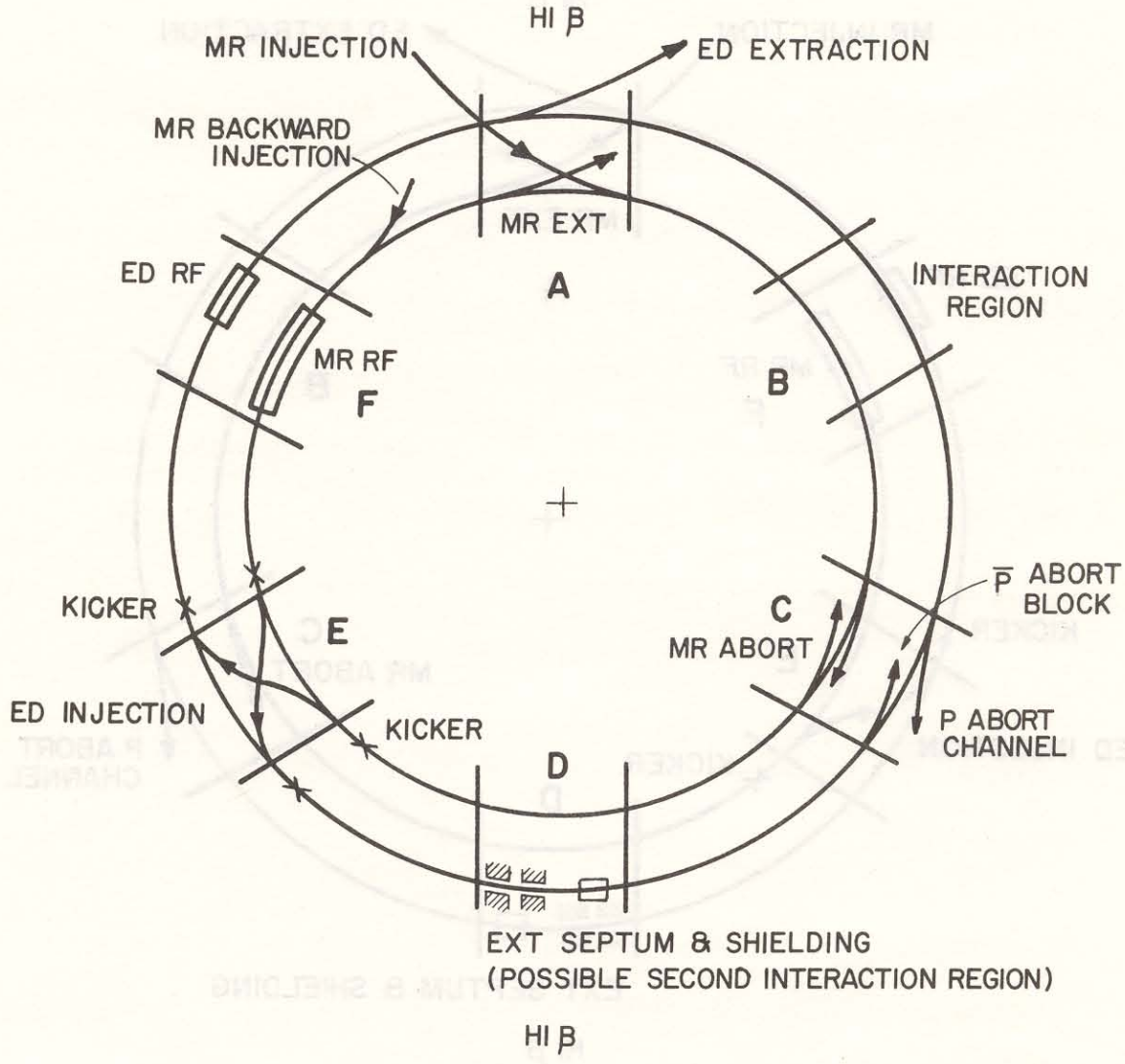

Fig. 1-3. Use of the six long straight sections in the colliding-beams mode.

increases on the superconducting-accelerator rf system, the demand on the Main-Ring rf system will probably reduce, so that putting the two rf systems in the same long straight section will provide optimum use of space for all times.

(ii) Since the extracted p beam has to go to the present switchyard, the extraction channel must be in A.

(iii) The electrostatic extraction septum should be at an odd number of quarter wavelengths of betatron oscillation upstream from the channel entrance in A. This proper phase occurs at F, D, and B. F is already occupied by the rf system; D is the next upstream and we therefore assign the extraction septum, and hence also the associated scraper-shield, to it. Detailed studies indicate that the beam loss on the septum will be about 30% more with the septum in D instead of in F. Nevertheless, the loss can be adequately shielded by the scraper-shield and the placement of the rf system in F is considered to have overriding merits.

(iv) It may happen that the p beam must be aborted during extraction. In this event, it is preferable to have the abort system located an odd number of quarter betatron-oscillation wavelengths upstream of the extraction septum, where the beam is narrower. Thus we place the abort systems in C. In so doing, we have reserved B, which is more easily accessible from the control room, for other functions needing more immediate and frequent access. The abort systems should not require as much access, at least during normal operation.

(v) Whether the easily accessible long straight-section B should be assigned to injection or colliding beams is largely a matter of choice.

We have chosen to locate the injection systems in E, leaving B for colliding-beams experiments. It would not cause any serious problem if the two functions were interchanged.

For a long period of colliding-beams operation with no fixed-target physics, it is conceivable that the extraction septum and scraper-shield at D could be removed and the straight section used as a second colliding-beams region. As will be evident later from the detailed discussions of the designs of beam-manipulating systems, there is no obvious way of shoehorning two of these functions into one long straight section to leave two straight sections permanently available for colliding-beams experiments.

In addition to these "lumped" systems in the long straight sections, there are "distributed" systems, each consisting of a large number of identical elements distributed around the ring, roughly one element to each mini-straight section. These are (1) the correction-magnet system, (2) the beam-detector system, and (3) the general scraper-shield system. These systems will also be described in detail in the following sections, as well as the major systems of the accelerator.

Parameters of the accelerator are collected in Appendix I for reference.

2. LATTICE

2.1 Ring Location and Normal Lattice

The design of the lattice of the superconducting ring is constrained by the requirement that it fit in the existing Main-Ring tunnel beneath the Main Ring. It is not realistic to consider any lattice that is not very similar to the Main Ring. The lattice designed therefore has 6 superperiods with 6 long straight sections and normal cells with 8 dipoles and 2 quadrupoles. There have been difficulties with magnet installation in the sector test because the superconducting dipole ends were directly under the Main-Ring ends and work space was extremely cramped. The bend magnets in this new lattice have therefore been moved 15.5 in. upstream. Figures 2-1a and 2-1b sketch the position of the quadrupole in the lattice and the position of a normal cell relative to the Main-Ring lattice. The beam center line will be 25.5 inches below Main-Ring center line.

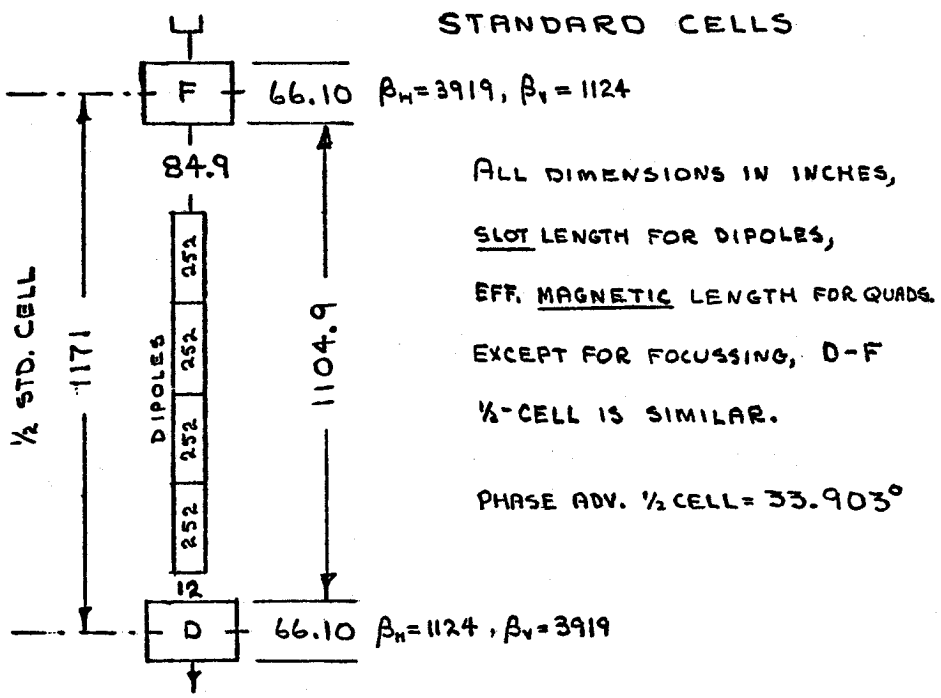

Fig. 2-1(a). Locations of elements in standard cell.

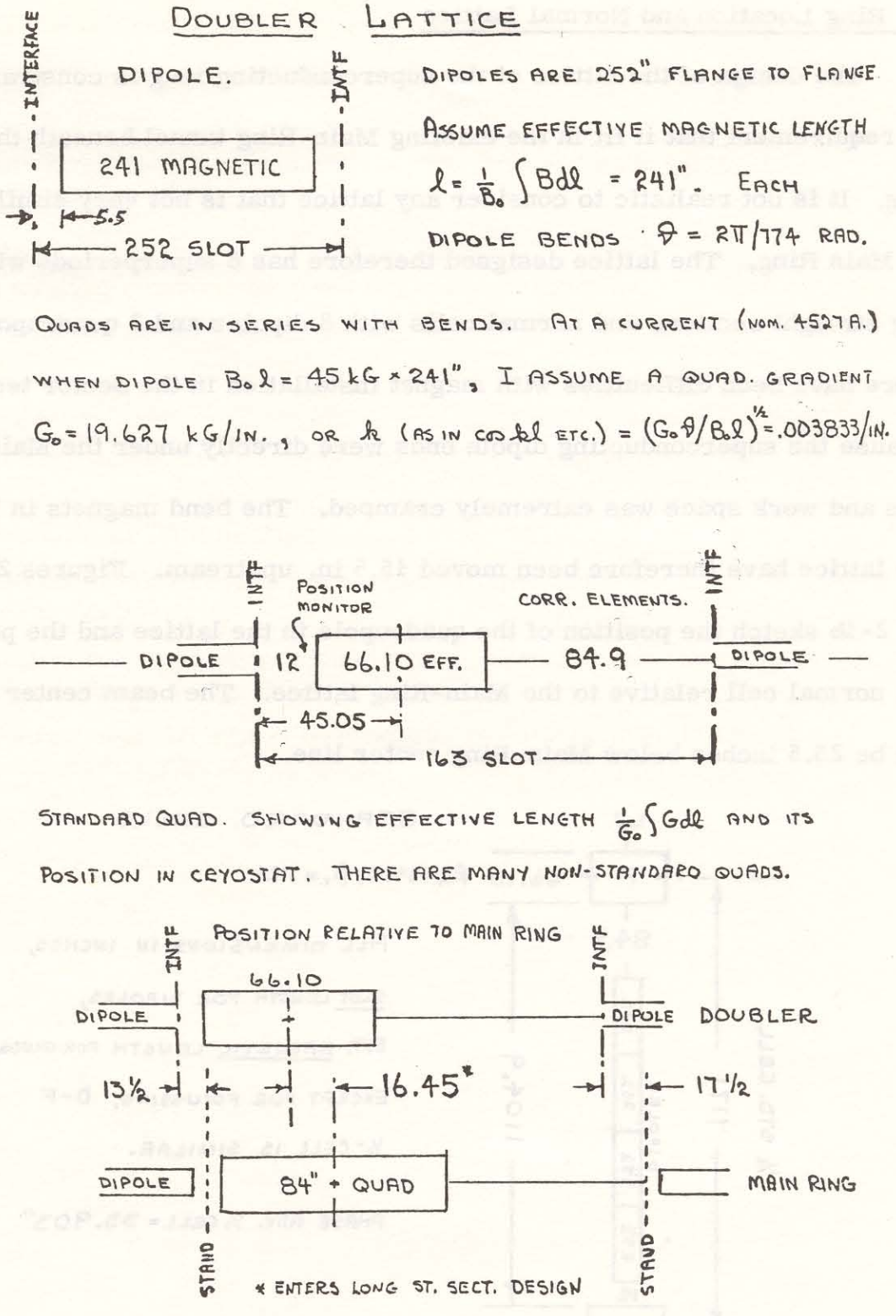

Fig. 2-1(b). Locations of superconducting magnets relative to main ring.

Like the Main Ring, the present lattice has a medium straight section at location 17 formed by omitting two dipoles. Its layout is shown in Fig. 2-1(c) below.

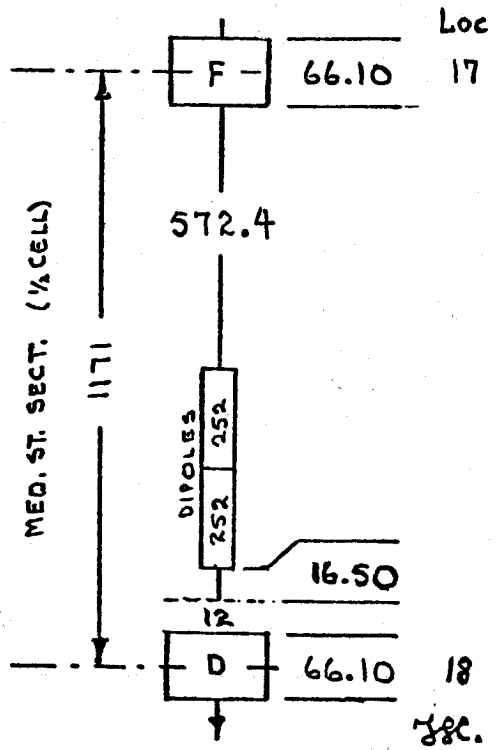

Fig. 2-1(c). Medium straight section. A std. $\frac{1}{2}$-cell with two dipoles omitted. A space of $16\frac{1}{2}$ inches must be inserted at downstream end to close the geometric orbit in the shifted Doubler.

There are also long straight sections of "normal" configuration, ones with high beta function for extraction, and ones with low beta for colliding-beam interactions. These will be discussed separately. Table 2-I summarizes the warm straight-section lengths available in the lattice. This table gives the drift lengths between "effective" magnetic ends of the elements, the available warm length and the space allotted for the cryogenic bypasses of cold-to-warm transitions and vacuum isolation. These bypasses will be discussed in Sections 4 and 5. All medium straight sections at 17 and 48 locations, as well as all long straight sections, will be warm. The space between the long straight-section doublets will be warm only where necessary.

2.2 Normal and High-Beta Long Straight Sections

Figure 2-2 is a sketch of the normal long straight section, giving lengths and amplitude functions. This design is very similar to that of the Main Ring, with the exception that two, rather than four, quadrupoles are

Table 2-I. Warm Straight-Section Lengths.

Location of Warm Region	Drift Length[a] (In.)	Available Warm Length (In.)	Hot-Cold Transition (In.) Upstream	Downstream
Median location 17 (standard quadrupole with corrections)	577.9	414.5	39	34
Normal-β median location 48	322.5	250.5	36	36
High-β median location 48	320.3	248.3	36	36
Normal-β doublet space 49, 11	150.36	78.36	36	36
High-β doublet space 49, 11	151.65	79.65	36	36
Long straight section	2094.25	2022.25	36	36
Low-β long straight section Type I	2046.25	1974.25	36	36
Low-β long straight section Type II	629.59	557.59	36	36

[a]Magnetic lengths used throughout to define drift lengths.

used at either end of the straight section. Normal geometry will be used at C0, E0, and F0. It will also be used initially at B0 before the low-beta quadrupoles are installed. Matching for injection between the Main Ring and the new ring can be easily accomplished with this geometry.

The high-beta long straight section is illustrated in Fig. 2-3. Here the order of focusing in the doublets has been reversed and lengths of all six quadrupoles changed slightly. A large horizontal beta is produced at the upstream end of the straight section. High-beta regions will be used at A0 and D0 to facilitate resonant extraction. The good-field aperture of the superconducting magnets is not large and the use of a high beta at the location of the extraction electrostatic and magnetic septa reduces the aperture required for extraction in the rest of the magnet ring.

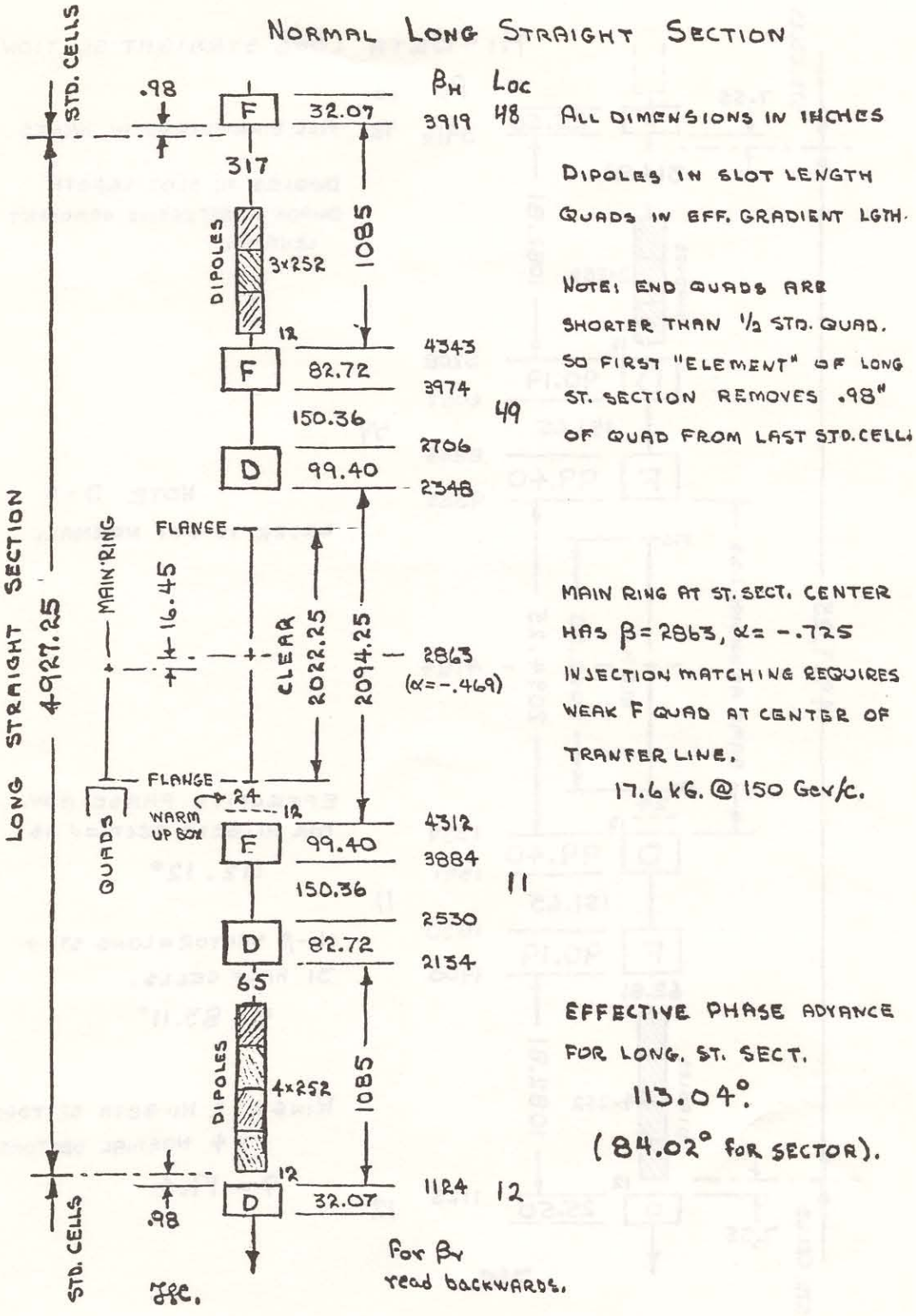
NORMAL LONG STRAIGHT SECTION
LONG STRAIGHT SECTION 4927.25
STD. CELLS
.98
F
32.07
317
DIPOLES
3×252
1085
12
F
82.72
150.36
D
99.40
FLANGE
MAIN RING
16.45
CLEAR 2022.25
2094.25
FLANGE
QUADS
24
WARM UP BOX
12
F
99.40
150.36
D
82.72
65
DIPOLES
4×252
1085
12
D
32.07
.98
STD. CELLS
β_H Loc
3919 48
4343
3974
49
2706
2548
2863
(α=-.469)
4312
3884
11
2530
2134
1124 12
ALL DIMENSIONS IN INCHES
DIPOLES IN SLOT LENGTH
QUADS IN EFF. GRADIENT LGTH.
NOTE: END QUADS ARE SHORTER THAN ½ STD. QUAD. SO FIRST "ELEMENT" OF LONG ST. SECTION REMOVES .98" OF QUAD FROM LAST STD. CELL.
MAIN RING AT ST. SECT. CENTER HAS β=2863, α=-.725
INJECTION MATCHING REQUIRES WEAK F QUAD AT CENTER OF TRANFER LINE.
17.6 kG. @ 150 Gev/c.
EFFECTIVE PHASE ADVANCE FOR LONG. ST. SECT.
113.04°
(84.02° FOR SECTOR).
For β_V read backwards.
Fig. 2-2. Normal long straight section.

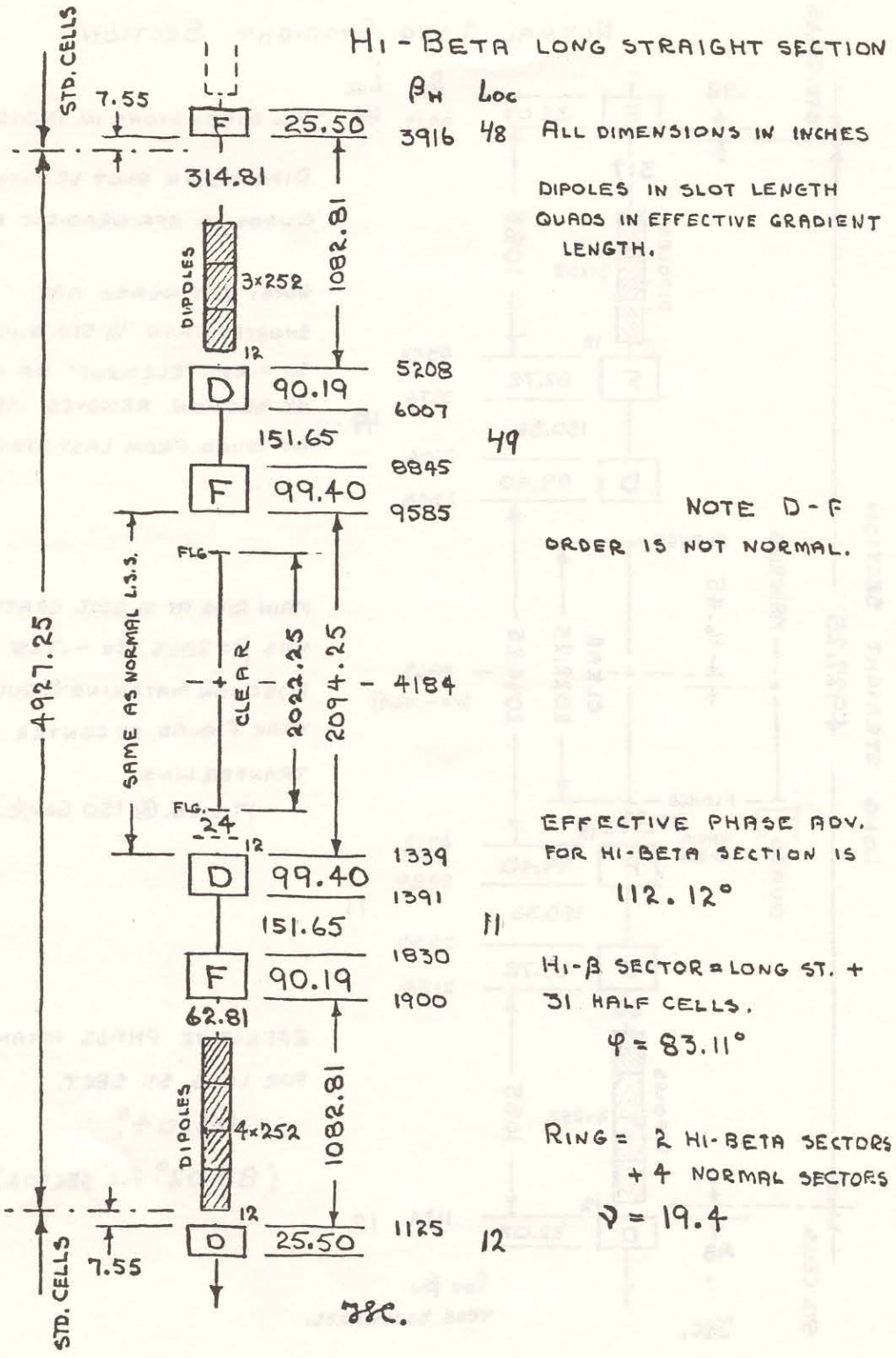

Fig. 2-3. High-beta long straight section.

We include in Appendix II a SYNCH output and geometrical drawings describing the lattice in detail without the low-beta section, which is treated separately in Section 2.5 below.

2.3 Circumference

In order to equalize the revolution times of unequal energy protons in the Main Ring, and the new ring for 150 × 1000 GeV pp colliding-beam physics, a slight increase in the path length of the higher energy beam is necessary. An effective change in path length could be made only using off-momentum orbits, but in view of the somewhat limited aperture in both rings, we have chosen to minimize the momentum offset necessary either at injection or during storage by making an increase in the circumference of the new ring of 4.4 cm. This value corresponds to an average $\Delta r/r$ increase of 7×10^{-6} relative to the Main Ring's 1 km radius.

This difference in radii will require the following operating conditions:

	Main Ring ($\Delta p/p$)	New Ring ($\Delta p/p$)
Injection	+0.25%	0.0%
150 × 1000 GeV pp	-0.32%	+0.10%

2.4 Lattice Elements

Table 2-II lists the various lattice elements required for a ring incorporating two high-beta long straight sections and four normal long straight sections. The lengths shown are magnetic lengths in inches.

2.5 Low-Beta Long Straight Section [1]

By replacing the two inner pairs of quadrupoles in the normal long straight section with considerably longer, independently powered, three-

Table 2-II. Lattice Elements.

Element	Magnetic Length (In.)	Number
Dipole	241.0	774
Standard quadrupole	66.1	180
Long straight inner quadrupole	99.4	12
Normal long straight short quadrupole (48, 12 location)	32.07	8
Outer quadrupole	82.72	8
High beta long straight short quadrupole (48, 12 location)	25.5	4
Outer quadrupole	90.19	4

shell quadrupoles, as shown in sketch (b) in Fig. 2-4, a pp colliding insertion can be produced. With the four outer quadrupoles running normally and the inner ones set at rather weak values, the lattice functions across this insertion can essentially duplicate those of the normal straight sections. By leaving quads #1 and #12 connected in series with the regular magnets, turning off quads #2 and #11, and repowering the inner quads, a β^* of approximately 10 m can be obtained. Quadrupole settings for these cases are listed in Table 2-III and some dynamic parameters are listed in Table 2-IV. Figure 2-5 illustrates the Type I interaction region. By adding additional power supplies to the other two pairs of quadrupoles, one can obtain lower values of β^*, although β_{max} starts to increase rapidly.

With the insertion of four more long, strong, and independently powered quadrupoles, one can produce a β^* of the order of 1 m. This is the Type II low-β shown in Fig. 2-4 and Fig. 2-6. Table 2-III lists quadrupole settings for minimum beta values of 1 and 2 m. Parameters for these cases are again listed in Table 2-IV. A few arbitrary decisions have been made at this point and should be mentioned.

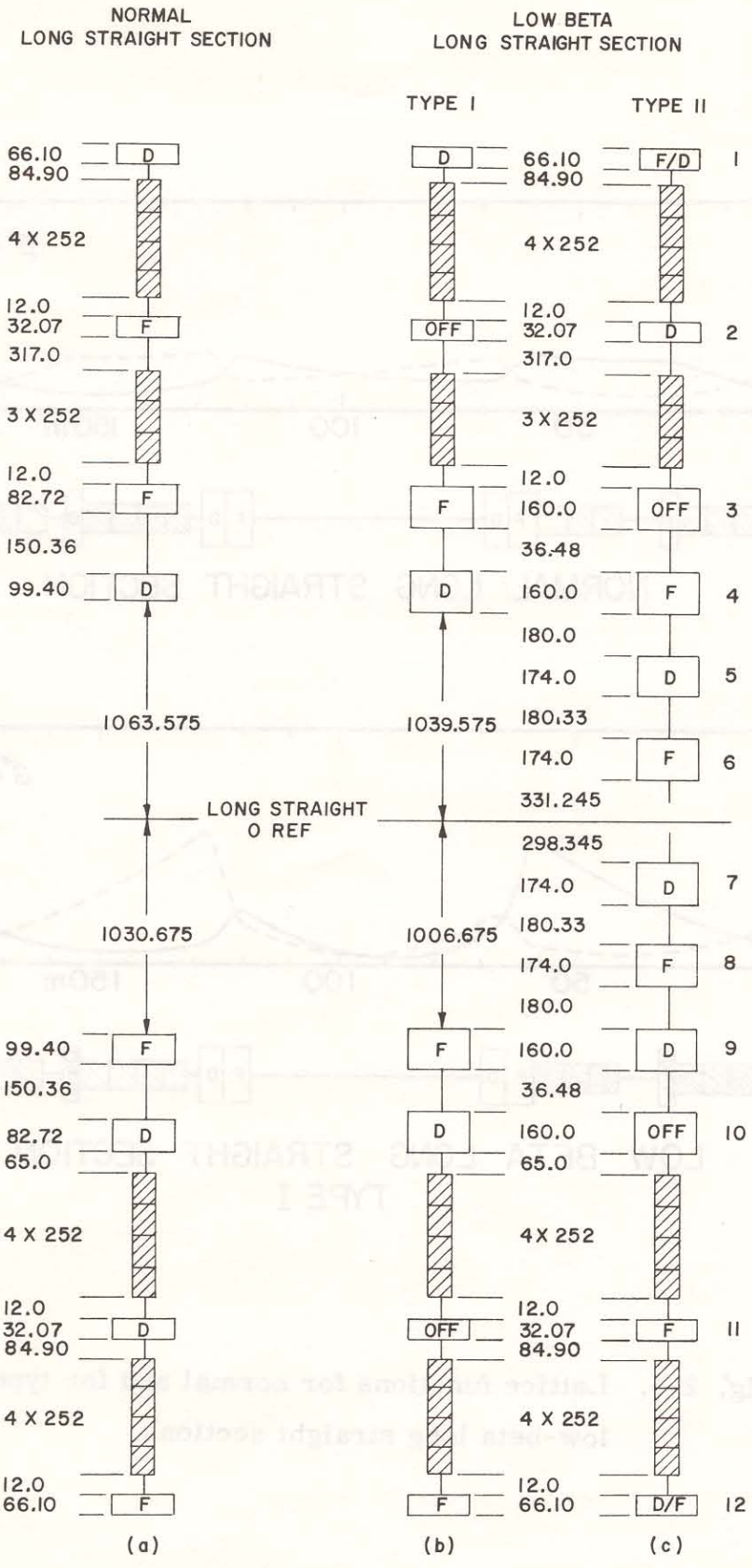

Fig. 2-4. Layout of normal and two types of low-beta long straight section.

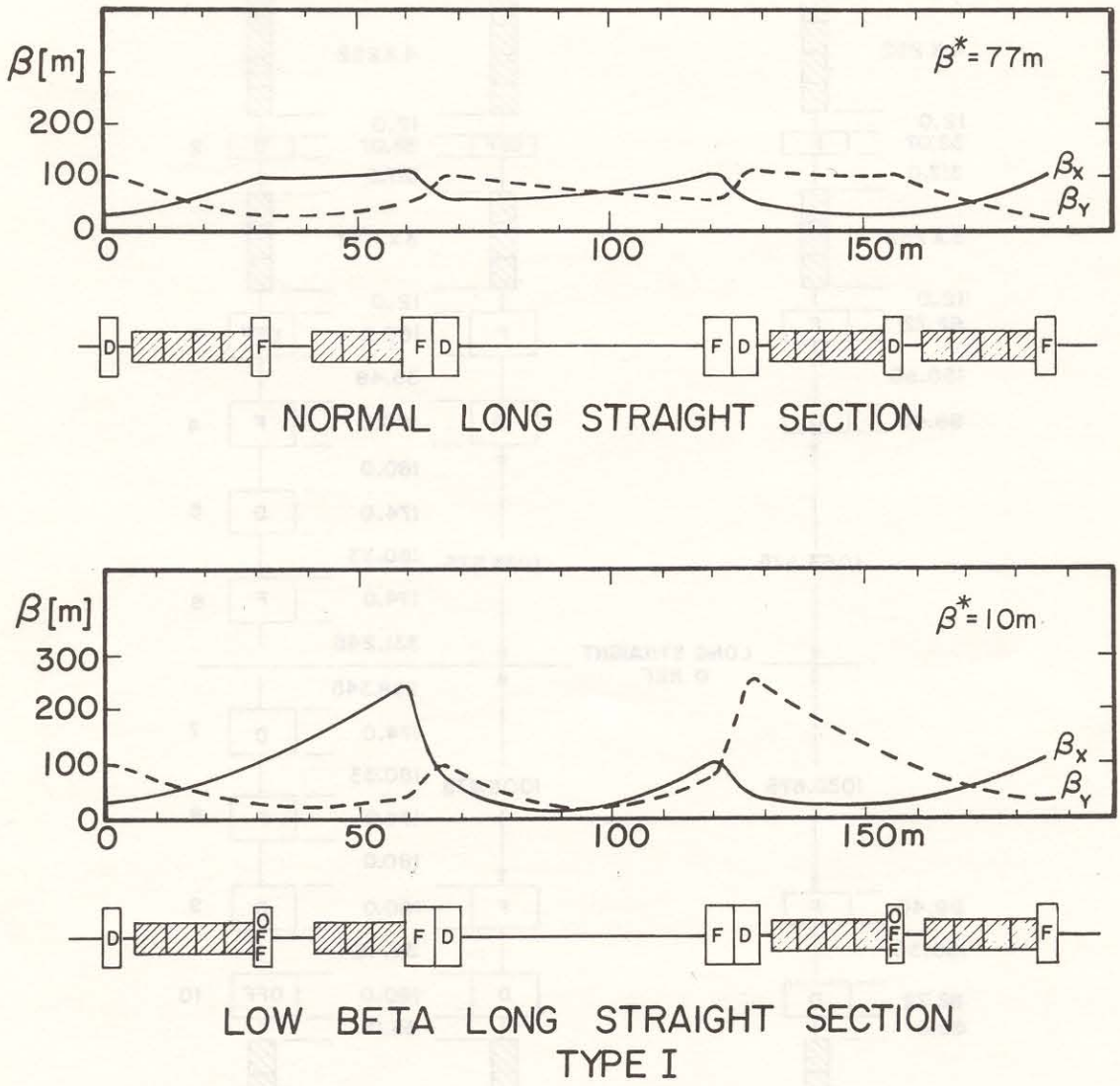

Fig. 2-5. Lattice functions for normal and for type I low-beta long straight sections.

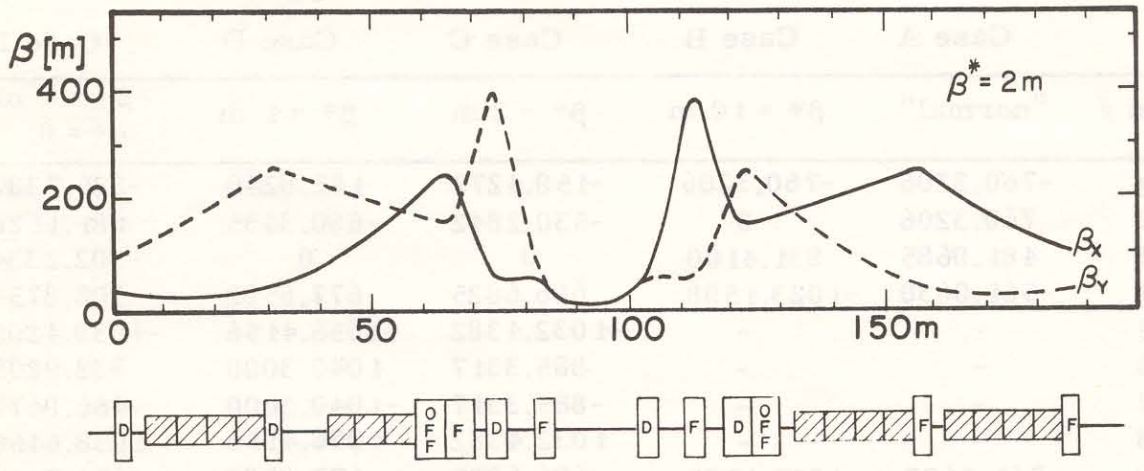

LOW BETA LONG STRAIGHT SECTION
TYPE II A

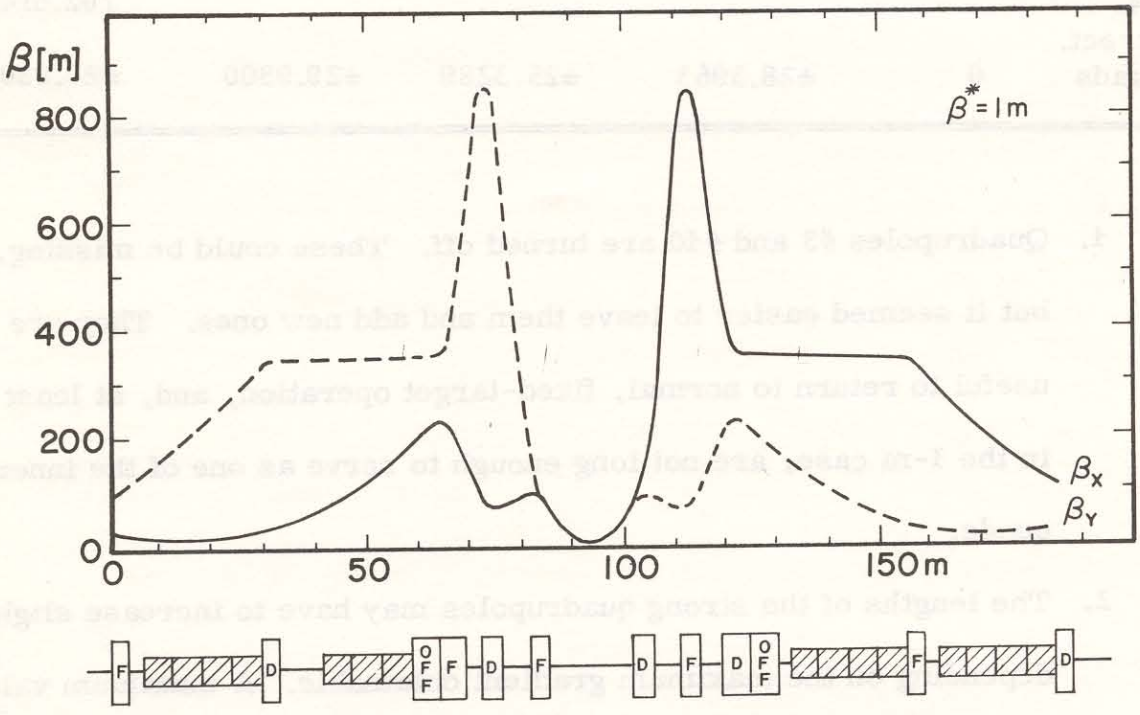

LOW BETA LONG STRAIGHT SECTION
TYPE II B

Fig. 2-6. Lattice functions for type II low-beta long straight sections.

Table 2-III. Quadrupole Settings (Values in kG/m for 1 TeV).

	Type I		Type II		
	Case A	Case B	Case C	Case D	Case E
Quad #	"normal"	$\beta^* = 10$ m	$\beta^* = 2$ m	$\beta^* = 1$ m	$\beta^* = 2$ m, $\eta^* = 0$
1	-760.3206	-760.3206	-159.4277	195.9240	-326.7387
2	760.3206	0	-530.2842	-690.3435	181.1120
3	481.9685	931.4100	0	0	-302.2334
4	-561.0630	-1023.1598	696.6825	677.6592	908.8754
5	-	-	-1032.4382	-1056.4156	-1039.4206
6	-	-	885.3317	1040.3000	932.9205
7	-	-	-885.3317	-1040.3000	-466.9477
8	-	-	1032.4382	1056.4156	1038.6460
9	561.0630	1023.1598	-696.6825	-677.6592	-654.7409
10	-481.9685	-931.4100	0	0	-75.5129
11	-760.3206	0	530.2842	690.3435	346.6425
12	760.3206	760.3206	159.4277	-195.9240	812.9308
13	normal	normal	normal	normal	-634.0335
14					702.6145
Correct. Quads	0	±28.3963	±25.3289	±29.9300	±29.9300

1. Quadrupoles #3 and #10 are turned off. These could be missing, but it seemed easier to leave them and add new ones. They are useful to return to normal, fixed-target operation, and, at least in the 1-m case, are not long enough to serve as one of the inner quads.

2. The lengths of the strong quadrupoles may have to increase slightly depending on the maximum gradient obtainable. A maximum value of approximately 26.8 kG/in. at 1 TeV has been used. Slight differences could be accommodated, perhaps down to around 25 kG/m, but certainly not as much as if one went to two-shell quadrupoles.

Table 2-IV. Lattice Functions.

	Normal lattice	Case A	Case B	Case C	Case D	Case E
Free Space (m)	53.194	51.974	51.974	15.992	15.992	15.992
β_x^* (m)	72.7	73.9	10.3	2.0	1.0	2.0
η^* (m)	2.24	2.26	0.21	0.40	0.48	-0.08
$\eta^{*\prime}$ (mrad)	18.1	18.2	-6.4	144	298	4.7
β_x max (m)	243	243	247	378	851	240
β_y max (m)	243	243	252	380	868	618
η max (m)	6.0	6.0	8.6	9.5	10.5	7.5
η min (m)	1.1	1.1	-0.5	-3.3	-5.2	-0.1
Q_x	19.395	19.393	19.394	19.393	19.400	19.632
Q_y	19.434	19.432	19.434	19.432	19.441	19.205
ξ_x	-22.5	-22.5	-23.2	-25.2	-29.1	-24.6
ΔQ of correction used	-	-	-0.317	-0.283	-0.334	-

Most of the objections raised with the previous low-β designs have been overcome in these designs. The maximum values of beta and dispersion have been brought down to believable sizes, and the dispersion mismatch throughout the ring is also relatively small. Further investigations of these designs show them to be quite reasonable. The tune corrections needed, from 30 correcting quads per sector, are easily handled, and the chromaticity corrections are also rather simple. Table 2-V lists the effect of momentum on various machine parameters for the low-β cases. The one parameter that could present a problem is the change in β_{max}. The percentage change of β_{max} as a function of $\Delta p/p$ is plotted in Fig. 2-7. Although this change in β_{max} is rather large, the correction system is the simplest possible, two independent sextupole families. By going to a larger

Table 2-V. Accelerator Parameters vs $\Delta p/p$.

β^* = 2 m,		$(B''\ell)_F$ = 429 kG/m,		$(B''\ell)_D$ = -733 kG/m	
$\Delta p/p$ (%)	β^* (m)	η^* (m)	η_{max} (m)	Q_x	Q_y
-0.375	1.76	0.36	9.3	19.394	19.434
-0.250	1.84	0.37	9.4	19.393	19.433
-0.125	1.92	0.39	9.5	19.393	19.433
0	2.01	0.40	9.5	19.393	19.432
0.125	2.10	0.42	9.6	19.393	19.433
0.250	2.20	0.43	9.7	19.393	19.433
0.375	2.30	0.44	9.7	19.394	19.434
β^* = 1 m,		$(B''\ell)_F$ = 492 kG/m,		$(B''\ell)_D$ = -842 kG/m	
-0.375	0.77	0.40	10.5	19.405	19.449
-0.250	0.84	0.43	10.4	19.402	19.444
-0.125	0.92	0.46	10.2	19.401	19.442
0	1.01	0.48	10.5	19.400	19.441
0.125	1.11	0.51	10.8	19.401	19.442
0.250	1.24	0.53	11.0	19.402	19.444
0.375	1.38	0.55	11.2	19.405	19.449

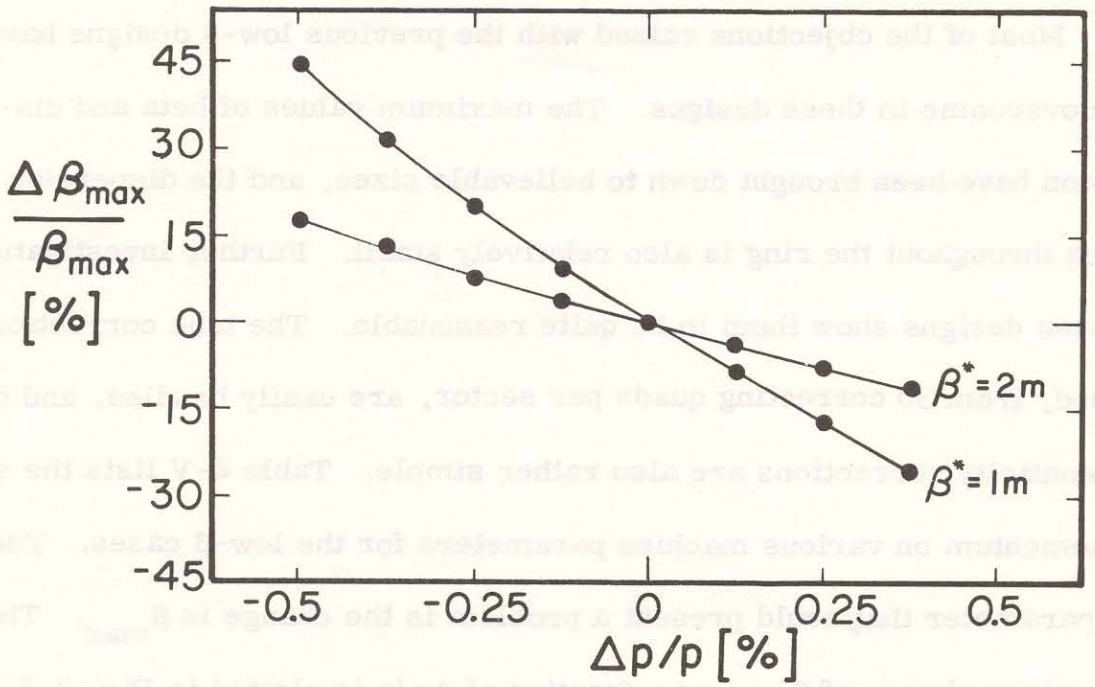

Fig. 2-7. Change in β_{max} as a function of $\Delta p/p$ for β^*=1m and β^*=2m.

number of circuits, a much smaller variation could be obtained. It should be noted that the momentum aperture discussed herein is for perfect magnets. Putting in design field distributions shrinks the available aperture considerably.

Finally, the question of non-zero dispersion at the collision point has been considered and a solution to overcome this problem has been found. This has not yet been studied in depth, but rather is presented as an existence proof. It consists of separately powering 14 quadrupoles, the 12 of Type II plus the next two downstream of the straight section, that is, those at stations 14 and 15. A plot of lattice functions for this case is shown in Fig. 2-8, and this is described in Tables 2-III and 2-IV, There are several points to be noted:

1. This was done for a 2-m β^*. An initial attempt to do it for 1 m failed.
2. The quadrupole at station 15 is definitely needed. Perhaps the one at station 14 could be run normally.
3. Quadrupole #12 is running too hard for a two-shell quad.
4. The tunes have not been properly rematched to 19.4. Completely making the dispersion zero is an extremely difficult process and may not be possible for other tunes.
5. The dispersion at the crossing point is shown as 8 cm. It can be made to be zero.

Finally, Fig. 2-9 is a layout of the interaction region at B0.

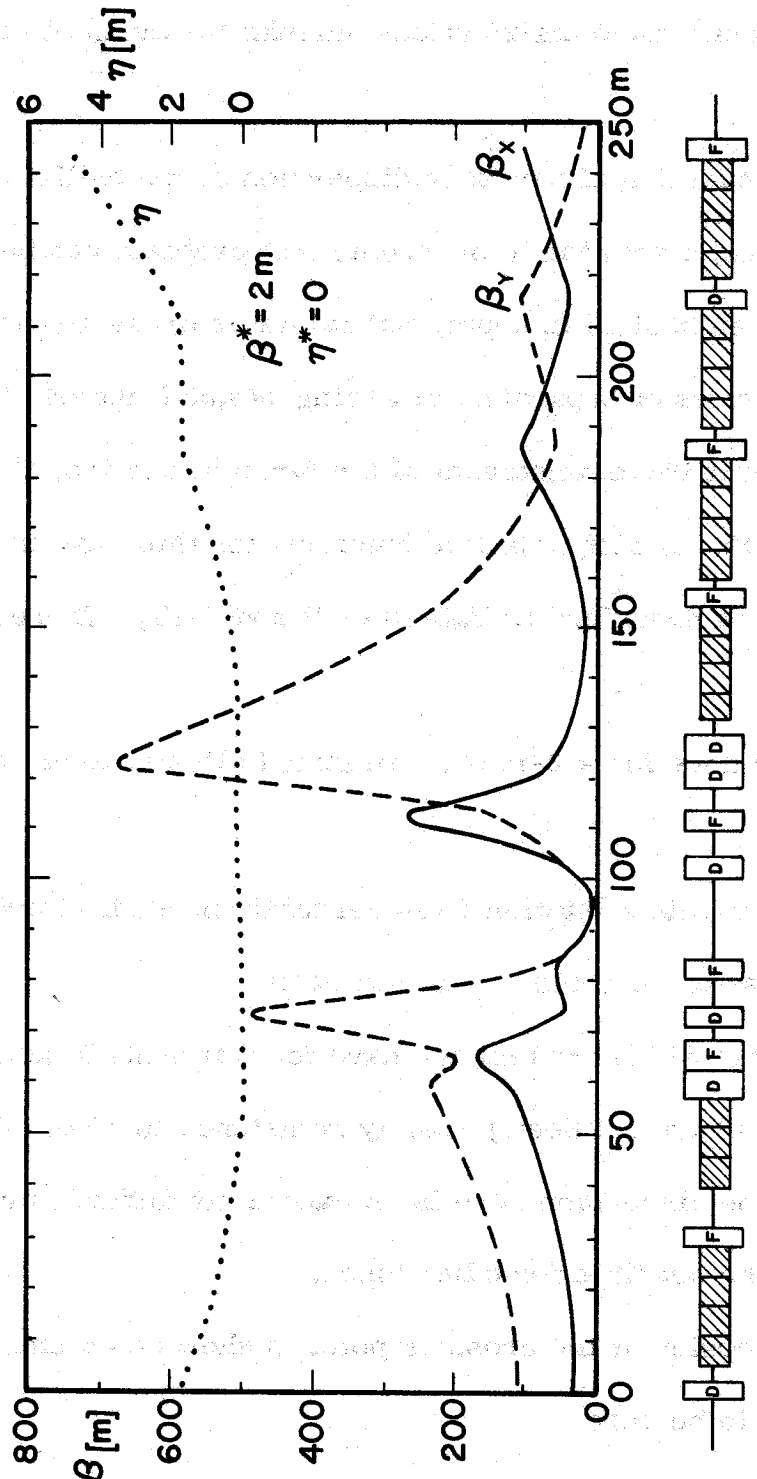

Fig. 2-8. Lattice functions for type IIC low-beta long straight section.

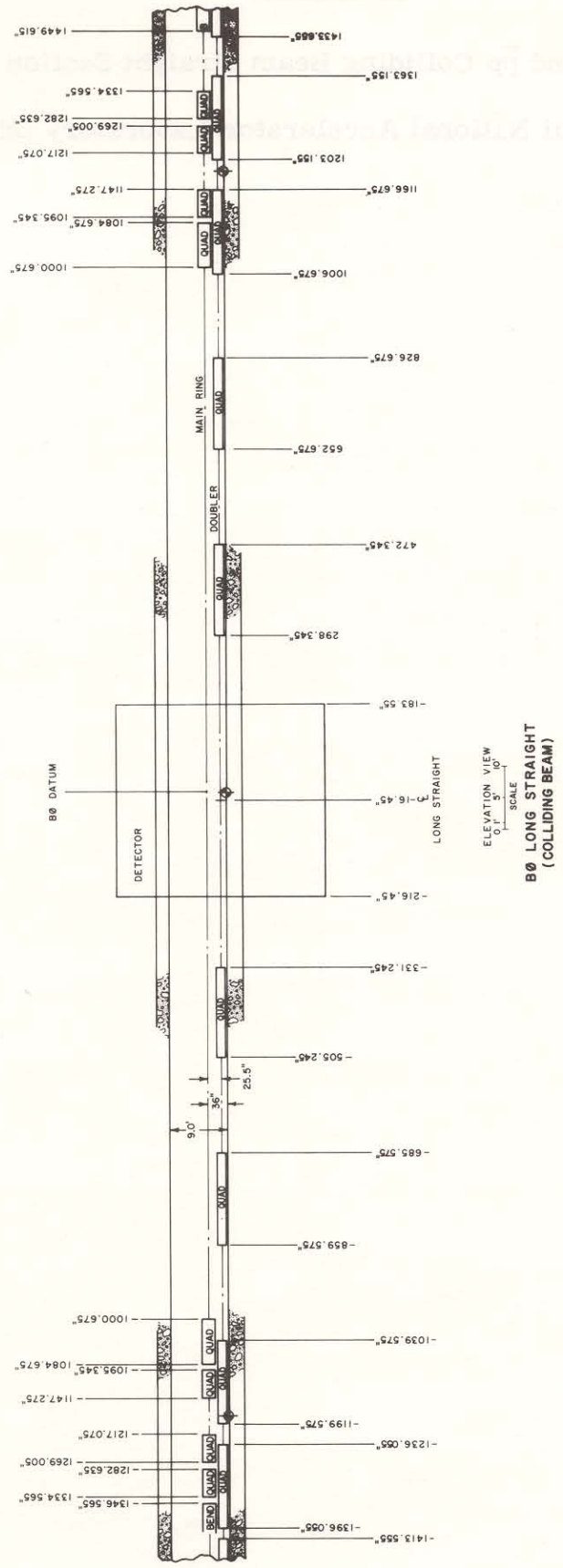

Fig. 2-9. Layout of the B0 long straight section.

Reference

[1] High Luminosity pp and $\bar{p}p$ Colliding Beam Straight Section Designs, D. E. Johnson, Fermi National Accelerator Laboratory Internal Report TM-876, April, 1979.